International Journal of Design & Nature and Ecodynamics
Vol. 20, No. 6, June, 2025, pp. 1203-1212
Journal homepage: http://iieta.org/journals/ijdne

Efficient Removal of Methylene Blue from Wastewater Using Co-Deposited $NiFe_3O_4/MgO/Cr_2O_3$ Nanocomposite Under Visible Light Irradiation

Ahmed Hameed Fayadh[1*], Shahlaa Esmail Ebrahim[2], Anmar Dherar Kosaj[1]

[1] College of Education for Pure Sciences, University of Anbar, Ramadi 31001, Iraq
[2] Environmental Engineering Department, College of Engineering, University of Baghdad, Baghdad 10071, Iraq

Corresponding Author Email: ahm23u3002@uoanbar.edu.iq

https://doi.org/10.18280/ijdne.200602

Received: 23 May 2025
Revised: 21 June 2025
Accepted: 25 June 2025
Available online: 30 June 2025

Keywords:
photocatalyst nanocomposites, MB degradation, visible-light irradiation (VL)

ABSTRACT

The photocatalysis method is an effective approach for removing environmental pollutants, particularly in the removal of dyes from wastewater, facilitating subsequent water reuse. In this work, three heterogeneous nanomaterials produced a co-sedimentation photocatalyst $NiFe_3O_4/MgO/Cr_2O_3$. This compound was characterized via FE-SEM, TEM, XRD, and FTIR. The spectra of the produced formulation revealed peaks in three regions that closely resembled the ranges identified in the individual components. This study focused on removing the organic dye methylene blue (MB) from wastewater to preserve water sources and aquatic life from toxic and carcinogenic pollutants. The effectiveness of MB degradation was examined under various conditions, including different photocatalyst dosages (0.5, 1, 2, and 3 g), initial pollutant concentrations (5, 10, 30, and 50 ppm), and pH values (2, 5, 7, and 11). About 97.5% of MB was removed by $NiFe_3O_4/MgO/Cr_2O_3$ with the reaction time (120 min) under the following optimal conditions: photocatalyst dosage of 1 g, MB concentration of 10 ppm, and pH 7. The heterogeneous triad composition $NiFe_3O_4/MgO/Cr_2O_3$ was created by producing each material separately and then co-depositing them. The XRD data showed that the peaks from $NiFe_3O_4/MgO/Cr_2O_3$ matched the original materials, but they were weaker. The data indicated a diffusion of materials piled on top of each other, resulting in signals from all components in the created composition, which was ideal. In comparison to the constituent parts utilized alone, the heterogeneous nanoparticles with the synthesized formula ($NiFe_3O_4/MgO/Cr_2O_3$) displayed a large surface area and a high rate of pollutant degradation (MB). When compared to applying each component alone, the combined efficacy of the produced combination ($NiFe_3O_4/MgO/Cr_2O_3$) was 97.5%. At the nanoscale, $NiFe_3O_4$ was 12% effective, MgO was 72% effective, and Cr_2O_3 was 64% effective. The effectiveness of the manufactured formula was demonstrated by these outcomes.

1. INTRODUCTION

The advancement in many chemical industries generates significant waste, including organic and inorganic residues, with dyes being the most critical, adversely affecting the environment and aquatic life [1]. Many dyes are used throughout multiple industries, including paper, textiles, and pharmaceuticals [2]. The presence of this pigment in wastewater or effluent from industrial areas significantly affects toxicity and has long-term implications for the environment and human health; thus, these environmental issues require a careful reconsideration to mitigate or eliminate their influence [3]. Previously, physical methods and absorption processes have been used to eliminate contaminants from wastewater due to their effectiveness and simplicity, but these processes have been demonstrated to adversely affect the environment, as they convert contaminated material from liquid to solid, necessitating additional disposal methods [4]. In this study, a method was employed to treat wastewater and eliminate numerous pollutants, including photosensitive dyes. This method is considered safe and environmentally benign because it uses natural energy sources, such as sunlight or artificial light from manufactured lamps, rendering it important and efficient [5]. Ordinary light, i.e., the lighting used in residential settings, has been used for photo stimulation, resulting in the degradation of pollutants in contaminated water through the presence of a catalyst [6]. Many nanomaterials have been used as photocatalysts to facilitate the removal of dyes or pollutants as a result of their unique properties that make them an important source in environmental remediation processes characterized by high efficiency, reduced time, and normal temperature, without causing water contamination [7].

From 2022 to 2025, notable advances have been made in the design of photocatalytic materials for the degradation of organic pollutants like methylene blue (MB), particularly under visible light irradiation. A major trend involves developing ternary and multi-component nanocomposites that

offer improved charge separation, redox activity, and visible-light utilization. For example, Vijayalakshmi et al. [8] successfully fabricated a Bi_2O_3/g-C_3N_4/ZnO nanocomposite that demonstrated enhanced photocatalytic degradation of MB, along with amoxicillin and chlorpyrifos. This system utilized a Z-scheme heterojunction mechanism, allowing efficient charge transfer and preservation of strong redox potentials. The material achieved high degradation efficiencies within 90 minutes under visible light, attributed to the synergistic interaction between Bi_2O_3, g-C_3N_4, and ZnO components.

Similar approaches have emphasized the role of band alignment engineering and electron transport pathways in ternary systems. For instance, composites involving ZnO, NiO, and MoO_3 or graphene oxide/g-C_3N_4/ZnO have shown significantly improved degradation rates for MB due to enhanced surface area, better dye adsorption, and suppression of electron–hole recombination [9]. These systems reflect a broader shift toward visible-light-active, stable, and recyclable photocatalysts for real-world wastewater treatment [10].

This growing body of research supports the rationale behind designing $NiFe_3O_4$/MgO/Cr_2O_3 nanocomposites. The incorporation of magnetic $NiFe_3O_4$ allows for easy post-treatment separation, MgO contributes to adsorption and surface alkalinity, and Cr_2O_3 enhances oxidative strength and structural stability. Such strategies align well with current efforts to optimize photocatalyst performance under sunlight while ensuring environmental and operational sustainability.

Ternary composite catalysts have some drawbacks that make them less useful in real life, even though they are more active and selective. One big problem is that it's hard to manage the composition and structure. It's hard to make a well-defined and homogenous ternary composite with the right component ratios, which makes the catalytic performance between batches inconsistent. Another issue is phase segregation, which can happen when some parts of a ternary system aren't stable together and may separate during synthesis or use. This makes the synergistic effects less effective. Also, optimizing flaws like oxygen vacancies that might boost catalytic activity is hard since it's hard to control their kind and density in the composite, and faults can affect various parts of the reaction in different ways, making it harder to optimize the reaction. Another problem with ternary composites is that they are too expensive because they contain rare or expensive materials like platinum, which are very good at catalyzing reactions but are not feasible for large-scale use. Ternary systems, like other catalysts, can also be poisoned by contaminants in the reaction mixture, which stops active sites from working and slows down the reaction. There are additional problems with selectivity because boosting catalytic activity in ternary systems doesn't necessarily lead to the required reaction selectivity. Finally, it's hard to figure out how specific structural elements affect catalytic performance because ternary composites have a complicated structure and composition. To get around these problems and make ternary composite catalysts more useful, we need to find ways to improve defect optimization, phase stability, cost, and selectivity. One way to do this is through lattice defect engineering, which could help support Cu-Mn-Ce composites work better and last longer.

Wang et al. [11] represented that one of the best ways to cut down on greenhouse gas emissions and make molecules with a lot of value is to hydrogenate CO_2 to methanol over Cu-based catalysts. There are certain problems with industrial CuZnAl catalysts; however, different promoters can make Cu-based catalysts for CO_2 hydrogenation work better and last longer. In this study, we looked at how different promoters changed the physicochemical properties of ternary CuZnM (M: Cr, Ce, Zr, Al) catalysts in a systematic way and how these changes affected the hydrogenation of CO_2 to methanol. The results show that the order of catalytic activity was CZCr > CZCe > CZZr > CZAl, with CZCr being the most stable of the four. Along with the results from XRD, SEM, TEM, H2-TPR, TPD, XPS, and Raman, the smaller Cu particle size helped to increase the yield of CH_3OH, and the lower Cu+/CuO ratio showed higher stability in the reaction of CO_2 with hydrogen to make methanol. This method gives us both theoretical knowledge and practical ways to use ternary Cu-based catalysts in industry.

Singh et al. [12] stated that the recent interest has focused on semiconductor-based hybrid materials' photocatalysis, energy applications, and environmental consequences. With a gap between 1 and 2 eV, Transition Metal Dichalcogenide (TMDSc) materials are ideal for two-dimensional materials. Simple microwave synthesis produced CdS/MoS_2/rGO. ternary composite SEM and XRD scans showed CdS/MoS_2/rGO in nanocomposite particles. Hexagonal CdS and MoS_2 crystals. CdS has a wavelength absorption peak of 514 nm and a bandwidth of 2.42 eV, while MoS_2 has 1.8–1.9 eV. CdS is 1 nm and MoS_2 is 500. Average nanocomposite size was 1 nm. This study tests sunset yellow dye's photocatalytic activity with ternary composite nanoparticles of CdS under visible light. Photocatalytic activity is affected by catalyst quantity, pH, dye concentration, and temperature. From 10 min to 180 min, the dye's degradation efficiency increases from 33% to 95%.

Despite these advancements, several limitations hinder the large-scale application of ternary composite photocatalysts. One of the main challenges is the complexity and high cost of synthesis, which often involves multiple preparation steps and sophisticated equipment. Additionally, achieving uniform dispersion and intimate interfacial contact among the three components can be difficult, affecting charge transfer efficiency and reproducibility [9]. Many ternary systems also face issues of photocorrosion, reduced stability under prolonged light exposure, or toxicity of certain components, which limits their environmental compatibility and recyclability. These drawbacks must be carefully addressed to realize practical, sustainable applications in wastewater treatment.

This research aimed to study the efficiency of the photocatalytic process in removing methylene blue (MB) dye from wastewater by synthesizing non-toxic composite nanomaterials that could effectively remove the contaminant under different operating conditions, including photocatalyst dosage, pollutant concentration, and pH.

2. MATERIALS AND METHODS

2.1 Materials

Nickel(II) nitrate [$Ni(NO_3)_2 \cdot 6H_2O$], iron(III) chloride [$FeCl_3 \cdot 6H_2O$], iron(II) sulfate [$FeSO_4$], ammonium hydroxide [NH_4OH], magnesium nitrate [$Mg(NO_3)_2$], sodium hydroxide [NaOH], chromium nitrate [$Cr(NO_3)_3 \cdot 9H_2O$], hydrochloric acid [HCl], ethanol [C_2H_5OH], and MB [$C_{16}H_{18}ClN_3S$] were used in this study. Materials with excellent analytical efficiency were used without any purification.

2.2 The process of light stimulation

Photocatalysis is a term composed of two parts: photo means light, and catalysis refers to stimulation; the stimulation process depends on the catalyst used in the chemical reaction without being altered by the catalyst's composition [13]. Photosynthesis involves four stages: the absorption of energy from light, excitation of electrons and a photonic stimulation reaction by using a light source where the photocatalyst absorbs light energy from the light source, transfer of the electron from the valence band to the conduction band across the energy gap, and generation of an electron–hole pair, as shown in Eq. (1) [14].

$$\text{Photocatalyst} + \text{light energy (hv)} \rightarrow e^- + h^+ \quad (1)$$

This process leads to the generation of hydroxyl radicals (•OH) by the interaction of water molecules with gaps, as shown in Eq. (2). The oxygen super roots (O_2^-) can be obtained through the interaction of electrons with dissolved oxygen, as in Eq. (3) [15]. Figure 1 shows the photocatalysis process under the influence of sunlight.

$$h + (VB) + H_2O \rightarrow \bullet OH + H^+ \quad (2)$$

$$e^- (\text{CB of PC}) + O_2 \rightarrow \bullet O_2^- \quad (3)$$

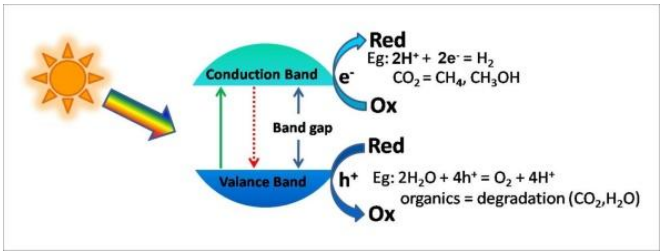

Figure 1. Photocatalytic process under the influence of sunlight

A photocatalytic batch reactor treats pollutants like methylene blue with two reactions: dark and light. This dark response is crucial to managing the process before adding light. The apparatus is kept in complete darkness to prevent photocatalytic activity. This stage allows pollutant molecules to solely adsorb on the catalyst. The reactor is always stirred, and the mixture is left in the dark for 30–60 minutes to establish adsorption–desorption equilibrium. This step determines how much pollutant the catalyst eliminates without light. This distinguishes physical adsorption from photocatalytic degradation. After the dark reaction and pollutant adsorption concentration are known, the light reaction begins. The reactor is then illuminated with visible or UV light to activate the photocatalyst. The catalyst absorbs photons, which transfer electrons from the valence band to the conduction band, leaving positively charged holes. These charge carriers then participate in redox processes that produce hydroxyl and superoxide radicals. These organisms react quickly to pollution molecules and break them down into carbon dioxide and water.

Pollutant concentration changes between dark and light phases show how well the catalyst decomposes contaminants photocatalytically. Without dark reaction data, it's difficult to establish if contaminants are eliminated by catalytic breakdown or surface adsorption. Thus, both phases are crucial to understanding a photocatalyst's performance and determining its efficiency. The control is important for figuring out how much of the pollutant removal (such as methylene blue) is caused by photocatalytic degradation in the light and how much is caused by passive adsorption onto the catalyst surface when there is no light. Adding measures like changes in concentration during dark adsorption equilibrium (about 30–60 minutes before irradiation) would help us better understand how the catalyst works and make the photocatalytic performance assessment more accurate.

The study examined the effectiveness of photocatalysis in breaking down MB dye in a one-liter Pyrex beaker used to make the mixture. The illumination of the reactor is achieved using a system of visible light sources, which includes four 30W xenon lamps. For the duration of the procedure, the photocatalysts were suspended in a mixture of MB dye and water. A pH that occurs naturally, 0.5 g of the generated photocatalysts, and a 100 ml solution of MB dye were all used in the first experiment. Ten parts per million was the starting concentration. The equilibrium between absorption and desorption was reached after 60 minutes. In the dark control, the mixture was constantly stirred [16]. The MB dye was then photocatalytically destroyed every 15 minutes for 120 minutes after the reactor was exposed to visible light. Figure 2 represents the batch reactor of the photocatalytic activity.

Figure 2. The batch reactor used in the photocatalytic degradation of MB dye

2.3 Photocatalysts

They are nanomaterials or micro semiconductors with exceptional light absorption properties, as certain materials may absorb light effectively without altering their structure throughout the reaction, leading to enhanced photocatalytic efficiency [17]. The photocatalyst possesses an equivalence band, identified as the highest occupied molecular orbital, and a conduction band, recognized as the lowest unoccupied molecular orbital. To achieve optimal efficiency, photocatalysts must incorporate catalysts effective in pollutant removal. Their features include a small energy gap, a large surface area, and low cost. Non-toxic chemicals may be reused in the decontamination process [18]. Several photocatalysts were used and selected based on the above-mentioned features. Three nanocides were identified: iron trioxide combined with nickel $NiFe_3O_4$, magnesium oxide (MgO), and chromium dioxide Cr_2O_3. These three materials were combined via chemical deposition and subjected to necessary tests.

2.4 The process of manufacturing nanoparticles

Nanomaterials are used in the environmental remediation process to facilitate the regulation of their volume and control their mechanical, electrical, magnetic, and optical properties [19]. Several methods can be used in the manufacture of photocatalysts, but this work employed co-deposition. This method is considered a chemical method that provides a straightforward means of producing nanomaterial oxides, thereby facilitating the creation of a triple composition of manufactured nanomaterials [20]. The heterogeneous triad composition $NiFe_3O_4/MgO/Cr_2O_3$ was achieved by a multi-step method, in which each material was produced separately and then assembled via co-deposition to form the desired composition. During the production process, $NiFe_3O_4$ was added to 2.2 g of $FeCl_3 \cdot 6H_2O$ and 1.6 g of $FeSO_4$, which were dissolved in 100 mL of deionized water. The mixture was agitated using a magnetic stirrer, after which drops of NH_4OH were added. The mixture was adjusted by 33% with the addition of 15 mL of deionized water, followed by an additional 60 mL for the NH_4OH drops. The color of the mixture turned black. It was allowed to sit for 20 minutes before introducing any other materials. Nickel was selected as a component of iron trioxide (Fe_3O_4), so we included 0.5 g of nickel into the mixture until thoroughly combined. After a certain period, we observed a color change in the mixture, indicating the successful blending of the two materials. The process was continued by including additional drops of NH_4OH, followed by the drying and washing of the resultant material, which produced a powder of $NiFe_3O_4$. Moreover, the coprecipitation temperature is between 22 and 25°C, and the stirring speed is around 400 rpm.

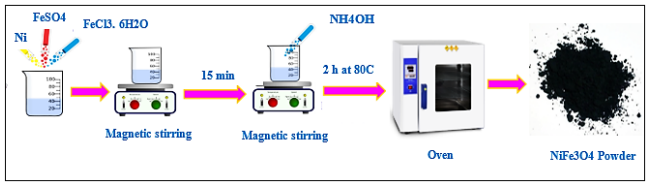

Figure 3. Stages of the $NiFe_3O_4$ production process

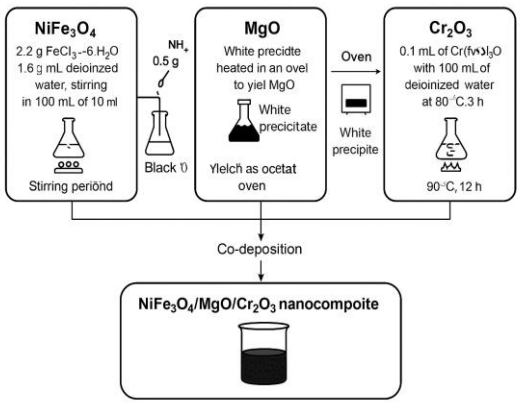

Figure 4. Schematic diagram of the Co-deposition synthesis process for $NiFe_3O_4/MgO/Cr_2O_3$ ternary nanocomposite

Figure 3 illustrates the production process of $NiFe_3O_4$. To produce MgO, we dissolved 7.5 g of magnesium nitrate in 50 mL of deionized water, and 10 g of sodium hydroxide was added to 250 mL of deionized water. The mixture was stirred for 30 min by using a magnetic stirrer at room temperature, during which a white precipitate formed at the bottom of the flask. This precipitate was then heated in an oven to yield MgO nanoparticles. During the synthesis of chromium trioxide, 0.1 mL of $Cr(NO_3)_3 \cdot 9H_2O$ was mixed with 100 mL of deionized water and subjected to magnetic stirring at 80°C for 3 h. The mixture was then transferred to an oven for 12 h at 90°C, followed by washing and drying to yield nanoscale Cr_2O_3. Figure 4 shows the diagram showing how the co-deposition synthesis process works for the $NiFe_3O_4/MgO/Cr_2O_3$ ternary nanocomposite.

3. CHARACTERIZATION OF SYNTHESIZED MATERIAL

Characterizing the newly synthesized photocatalysts required the use of a number of different techniques, such as "XRD, FE-SEM, TEM, and FTIR." The “XRD” investigation was carried out at a temperature of 25 degrees Celsius with an X-ray diffractometer made by Shimadzu called the XRD-7000, graphite-chromatized Cu K radiation with a wavelength of 0.15418 nanometers, a tube voltage of 40 kilovolts, and a current of 30 milliamperes. The “field emission scanning electron microscopy” (FE-SEM) (Tescan Mira 3) was utilized with the purpose of studying the produced photocatalysts' morphological structures. The Hitachi U-3900H instrument was used for this research. The morphological features and sizes of the man-made nanoparticles were investigated with the help of a scanning electron microscope (SEM). Fourier Transform Infrared Spectroscopy (FTIR) is a method that measures how materials absorb infrared light to find functional groups and chemical bonds. When IR light goes through a sample, certain bonds vibrate and take up energy at certain frequencies, which makes a spectrum.

FTIR shows the production of metal–oxygen bonds, finds impurities, and proves that the composite was successfully made in nanomaterials like $NiFe_3O_4/MgO/Cr_2O_3$. It's a quick and safe approach to see if the right structure was made.

The characteristics were done by Hesgar Mavad Saba (HMS) Research Lab, Islamic Azad University, Tehran, Iran.

4. RESULTS AND DISCUSSION

4.1 X-ray diffraction (XRD)

XRD analysis was conducted to determine the crystal structure and grain size of the composite fabricated by co-precipitation of $NiFe_3O_4/MgO/Cr_2O_3$. This test offers a technique for determining the properties of nanomaterials and solids without affecting the composition of the material. When X-rays interact with the target material, a diagram is produced that represents the identity of that material, thereby providing information about it [21, 22]. Figure 3 shows an XRD image. We observed the peaks of MgO at 2θ angles of 42.8° and 62.2°, and the observed values were consistent. The diffraction peaks of the nanoparticles were attributed to 200 and 220, respectively. Meanwhile, Cr_2O_3 exhibited a prominent peak at 26.99°, with additional peaks present but of minimal intensity, corresponding to the diffraction levels of the nanoparticles, specifically (012). For $NiFe_3O_4$, its peaks emerged at the 2θ angles of 29.9°, 33.1°, 36.6°, 39.2°, 52.2°, 57.9°, and 60.3°, in accordance with the international standards [23]. The peaks at 29.9°, 33.1°, 36.6°, 39.2°, 52.2°, 57.9°, and 60.3° were

attributed to the indices at 220, 311, 222, 400, 422, 511, and 440 of $NiFe_3O_4$, respectively. The peaks or signals that appeared in $NiFe_3O_4/MgO/Cr_2O_3$ were consistent with the constituent materials used in this production, but with diminished capacity. This suggested a dispersion of the materials layered upon one another, resulting in the appearance of signals from all components within the manufactured composition, which was deemed optimal [24].

The XRD study shows that the individual metal oxides—$NiFe_3O_4$, MgO, and Cr_2O_3—were successfully made and that they are structurally sound. It also shows that they may be combined to make the ternary $NiFe_3O_4/MgO/Cr_2O_3$ nanocomposite. Figure 5 clearly shows the distinctive diffraction peaks of each oxide, which means that no undesired secondary phases have formed. The Debye–Scherrer equation was used to figure out the diameters of the crystallites in the materials that were made.

$$D = (K\lambda) / (\beta \cos \theta)$$

where,

D is the average crystallite size,

K is the Scherrer constant (typically 0.9),

λ is the X-ray wavelength (1.5406 Å for Cu Kα),

β is the full width at half maximum (FWHM) of the diffraction peak (in radians),

θ is the Bragg angle (in degrees).

These nanometer-scale sizes show that nanocrystalline materials with possible photocatalytic and adsorption properties have been made. The fact that the crystallite sizes are quite similar among the three oxides shows that they can be combined to make a useful ternary nanocomposite. We used this formula to figure out the sizes of the crystallites that made up the biggest peaks of each oxide. The average size of the $NiFe_3O_4$ crystals was around 27.1 nm. The diameters of the MgO and Cr_2O_3 crystals were about 34.3 nm and 28.7 nm, respectively. These sizes, which are in the nanometer range, show that nanoscale crystals have formed, which is necessary for photocatalytic or adsorption applications that need a lot of surface area and reactivity. The fact that the crystallite sizes are all rather near to one another also shows that these phases can work together in the composite system.

Table 1. Crystallite size estimation of $NiFe_3O_4$, MgO, and Cr_2O_3 phases based on XRD analysis using the Scherrer equation

Material	2θ (°)	Plane (hkl)	FWHM (°)	Crystallite Size (nm)
$NiFe_3O_4$	35.7	311	0.30	27.1
MgO	43.2	200	0.25	34.3
Cr_2O_3	33.5	104	0.28	28.7

Table 1 shows the results of the XRD analysis for the three phases—$NiFe_3O_4$, MgO, and Cr_2O_3—that made up the ternary nanocomposite. The Scherrer equation was used to find the average crystallite size for each oxide by looking at the most intense diffraction peak. The 2θ values show the main diffraction peaks, while the FWHM (full width at half maximum) values show how the peaks spread out, which is the opposite of the crystallite size. The calculated crystallite sizes for $NiFe_3O_4$, MgO, and Cr_2O_3 were about 27.1 nm, 34.3 nm, and 28.7 nm, respectively. These values confirm that all three phases are nanocrystalline, with slight differences in size due to differences in structural properties and synthesis conditions. The particles' consistent nanoscale dimensions suggest that the synthesis process was successful and give the material a larger surface area, which is good for photocatalytic and adsorption applications.

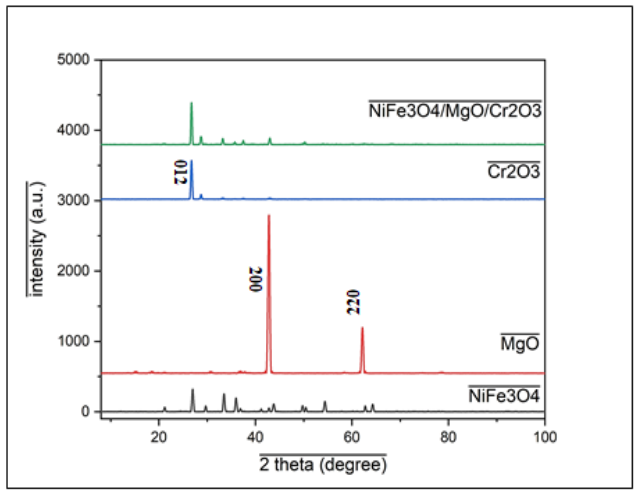

Figure 5. XRD image of three nanomaterials and their combination

4.2 Field emission scanning electron microscopy (FE-SEM)

FE-SEM analysis is a crucial test for monitoring the surface of the sample and identifying nanoparticles, thereby clarifying some of the defects present in the examined sample [25]. The obtained images revealed the presence of three nanomaterials, each varying in shape and concentration, observed at magnifications of 120 and 30Kx. Figure 6 shows FE-SEM images of the prepared overlay $NiFe_3O_4/MgO/Cr_2O_3$. The $NiFe_3O_4$ nanoparticles exhibited spherical or semi-spherical morphologies. MgO appeared in irregular hexagonal forms and had a distinct color, predominantly white, which facilitated its differentiation from the other materials. Cr_2O_3 appeared as small, light black tubes that overlapped with the other components utilized in the formulated product.

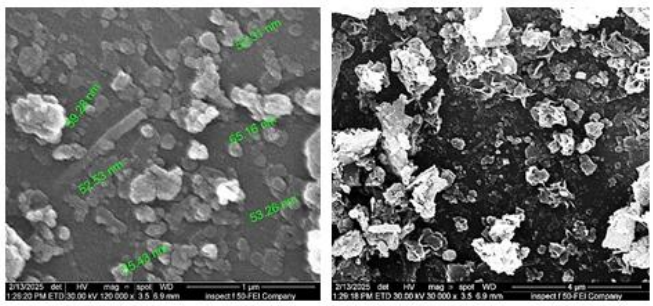

Figure 6. FE-SEM analysis of the prepared composite ($NiFe_3O_4/MgO/Cr_2O_3$)

4.3 TEM

Transmission electron microscopy was conducted to study the crystal structure, surface shape, and particle shape and size of the sample [26]. The ternary structure of $NiFe_3O_4/MgO/Cr_2O_3$ was analyzed. The images in Figure 6 show this combination of the three oxides. The high magnification power of these images revealed intricate details of the materials used in this combination, highlighting the

presence of clusters of MgO and Cr_2O_3 on $NiFe_3O_4$. In certain areas, chromium trioxide was superimposed on $NiFe_3O_4$. MgO exhibited hexagonal and transparent structures, whereas Cr_2O_3 presented as light black tubes or rods intertwined with $NiFe_3O_4$ and occasionally with MgO. $NiFe_3O_4$, a dark black compound, was interspersed with MgO and Cr_2O_3.

The TEM picture of the $NiFe_3O_4/MgO/Cr_2O_3$ nanocomposite shows that it has a mixed form, with clusters of particles that are not all the same size and shape. The changes in contrast seen in the picture suggest that there is more than one phase, which means that the three metal oxides were successfully combined. The particles are mostly less than 100 nm in size, and some of them look like plates or rods, which is what other studies have found in mixed metal oxide systems. The particles may have stuck together because of magnetic interactions between the $NiFe_3O_4$ domains or because the samples were dried before they were prepared. Without a particle size distribution map, nevertheless, it is still hard to make a quantitative estimate.

We used contour analysis to guess the sizes of the particles and the scale bar (100 nm) to make sure they were correct. Most of the particles are between 25 and 50 nm, but a few are bigger, up to 160 nm. This shows that the sample is mostly polydisperse and has mostly nanoscale characteristics, which supports the idea that nanostructured materials are being made. The distribution we saw supports the idea that there are particles in the expected nanoscale range and matches the expected shape from TEM examination. Figure 7 shows the TEM of the composite.

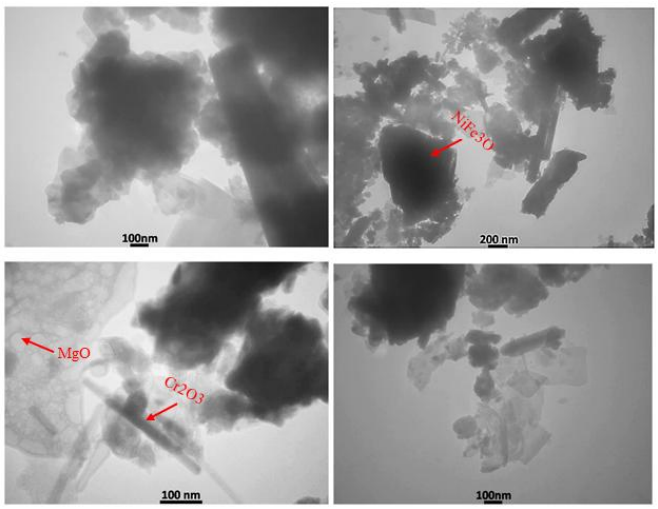

Figure 7. Detailed images of the composite material comprising the nanomaterials $NiFe_3O_4$, MgO, and Cr_2O_3

4.4 FTIR analysis

FTIR was conducted within the range of 500–4000 cm^{-1}. Figure 8 shows the infrared spectrum of the compound $NiFe_3O_4/MgO/Cr_2O_3$ and its components. The infrared spectrum of the material showed that MgO had four bands scattered along the spectrum, including a broad band in the region of 1500–3500 cm^{-1}, a band at 570.22 cm^{-1} corresponding to the Mg-O bond, and another at 1436.8 cm^{-1}. The range was 3418.2–3693.5 cm^{-1}. Hydroxide groups appeared as OH. The infrared spectrum of $NiFe_3O_4$ nanoparticles exhibited six distinct bands distributed throughout the spectrum. Hydroxyl radicals were detected at three specific wavelengths: 3411.8, 1622.7, and 1031.4 cm^{-1}. The other ranges were 1388.9, 914.15, and 542.2 cm^{-1}, which represented simple vibrations along the axis. The spectra of Cr_2O_3 exhibited loss in bundles throughout four regions, and hydroxyl radicals were detected within the range of 1381.7–1024.2 cm^{-1}. However, within the range of 914.1–542.2 cm^{-1}, several vibrations appeared, consisting of CO-O in that area. The infrared spectrum of the composite material $NiFe_3O_4/MgO/Cr_2O_3$ closely resembled that of the individual components, indicating that the resulting spectrum was the sum of the bands present in the three materials combined. The beam group represented active sites where the absorption process occurred [27].

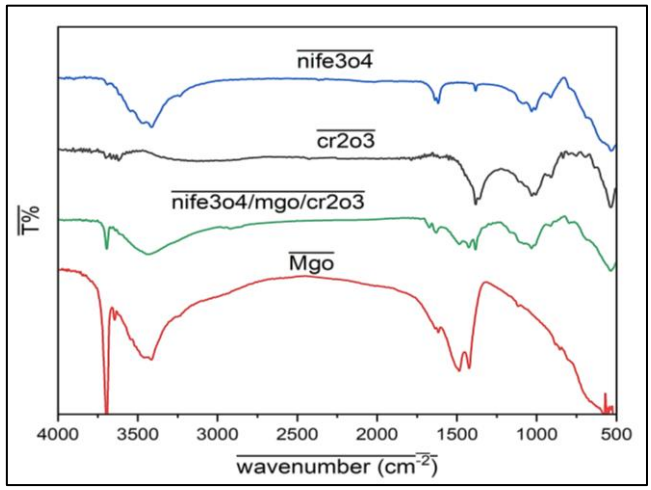

Figure 8. FTIR spectra of $NiFe_3O_4/MgO/Cr_2O_3$ and its components

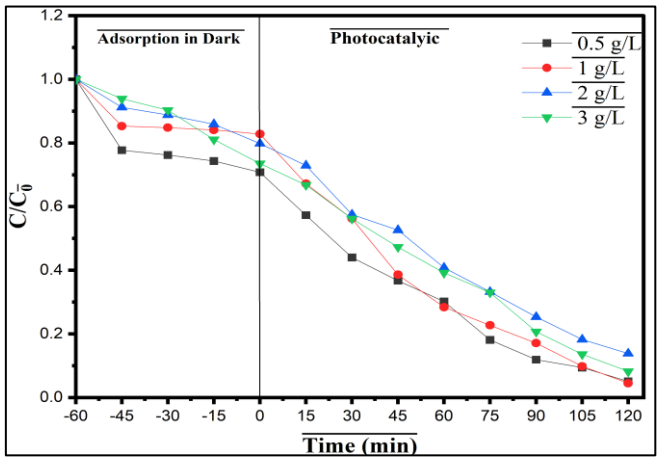

Figure 9. Photocatalyst dose and its effect on the removal process of MB

4.5 Degradation of MB dye

4.5.1 Effect of photocatalyst dose

The photocatalyst plays an important role in the MB dye removal process. Different doses of the catalyst were used, namely, 0.5, 1, 2, and 3 g. Figure 9 shows the concentrations of the photocatalyst, indicating the concentration at which the optimal removal efficiency for MB dye was achieved, namely, a pollutant concentration of 10 ppm and pH 7. The highest removal efficiency occurred at a concentration of 1 g. During the absence of light, the removal efficiency was very low and stable at all times. However, the removal efficiency changed after light exposure, indicating the strong effect of light on the

degradation of the dye in the water. The other catalyst concentrations demonstrated effective removal, but with a lower efficiency compared with the concentration established at 1 g. The combination of the catalyst color and the dye color resulted in high opacity, which impeded light penetration into the dye, thereby leading to less efficient degradation of the dye [28].

4.5.2 Effect of the MB concentration

Four concentrations of MB dye were selected. The concentrations selected for comparison in this study were 5, 10, 30, and 50 ppm. Figure 10 shows the concentrations of the pollutant (MB) and the optimal concentration that had the maximum removal efficiency. The test was carried out with a photocatalyst concentration of 1 g/L at pH 7, where the focus indicated 10 ppm. The pollutant concentration of 5 ppm demonstrated high efficiency compared with the other concentrations (30 and 50 ppm). The difference in the removal efficiency among the tested concentrations was attributed to the degree of darkening associated with each dye concentration, as the extent of darkening differed across samples, thereby affecting the dye removal process within the designated time frame [29]. The maximum duration was 120 min, resulting in a difference in dye removal efficiency (MB) across various concentrations.

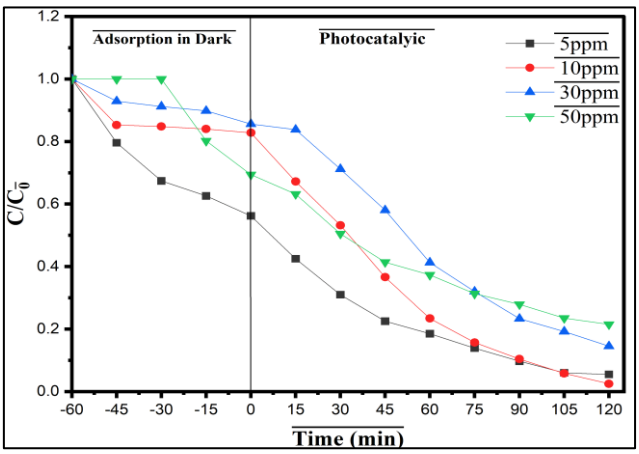

Figure 10. Concentrations of MB dye and their effect on removal efficiency

4.5.3 Effect of pH

The pH is an important factor affecting the photocatalytic process; thus, it was considered in all tests because of its role and efficacy in pollutant removal [30]. Figure 11 shows the correlation between pH values and pollutant removal efficacy. Four pH values were selected, namely, pH 2, pH 5, pH 7, and pH 11. These values were compared in terms of the removal efficiency of the dye pollutant (MB) at each value, with the photocatalyst set at 1 g. The pollutant concentration was 10 ppm. The analysis indicated that optimal clearance was achieved at pH 7. The remaining values may not be accepted. Significant convergence was observed in the removal value between pH 2 and pH 5. The removal was highly stable at pH 7. However, at pH 11, the removal efficiency was inferior compared with the other values. This outcome was attributed to the interaction of hydroxide ions with the roots to generate hydroxide radicals, which delayed the process of decomposition at elevated pH levels [31]. Despite the difference in removal efficiency across all values, we obtained the removal efficiency for each individual value. The removal efficiency was determined to be 97.5%. At pH 7, the pollutant concentration was 10 ppm, and the concentration of the photocatalyst was 1 g.

The produced $NiFe_3O_4/MgO/Cr_2O_3$ composite had a photocatalytic degradation efficiency of 97.5%, which puts it in the same league as well-known photocatalysts like ZnO/TiO_2. For example, Zha et al. [32] created nanostructured TiO_2/ZnO heterojunctions that broke down about 97% of methyl orange in 30 minutes when exposed to UV light [32]. In the same way, Zhang et al. [33] found a ZnO/TiO_2 system that could break down 98.6% of its components under a 36 W UV light for 300 minutes and still work at more than 90% efficiency after five reuse cycles [2]. Dai et al. [34] created a $TiO_2/ZnO–NH_2$–reduced graphene oxide composite that had a photocatalytic rate 3.2 times greater than TiO_2/ZnO alone. This was because the composite had better charge separation and adsorption capabilities [33]. The $NiFe_3O_4/MgO/Cr_2O_3$ composite not only breaks down at a similar rate as these other materials, but it also has the potential for magnetic separation and better recyclability because it contains magnetic and basic oxides. These results show that the existing composite works quite well and can be used in real life for enhanced wastewater treatment.

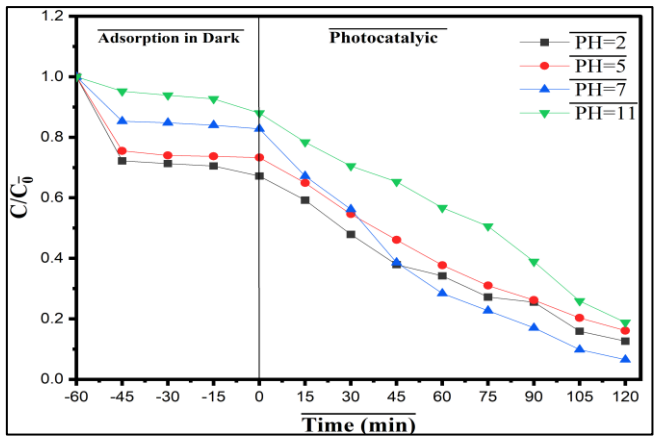

Figure 11. pH values and their effect on the removal of MB dye

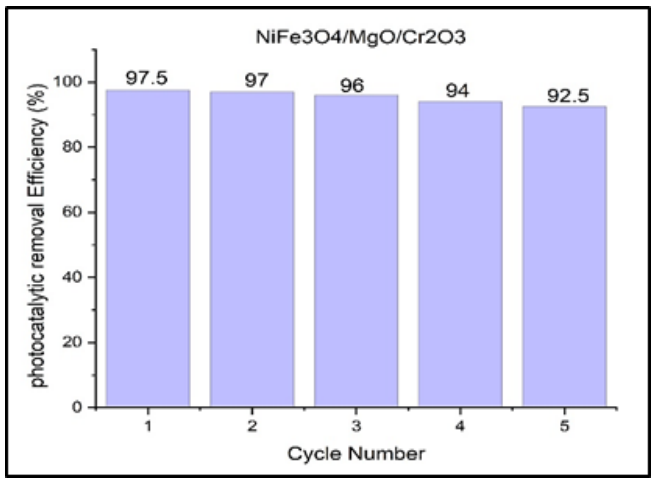

Figure 12. Synthesized photocatalysts' stability and reusability over five operating cycles at MB dyes

4.5.4 Study on the possibility of reuse

The manufactured nanocomposite was used for more than one cycle to assess its efficiency in removing the contaminant

methylene blue (MB) dye. The removal efficiency was tested in each removal cycle, which lasted 120 minutes. After each cycle, the material was washed with ethanol and distilled water, then dried and reused. The material was used for five cycles, and it was observed that the removal efficiency in the first cycle was high, reaching 97.5%. It was noted that the removal efficiency gradually decreased after each cycle, which indicates a loss in the mass of the photocatalyst [26]. This reduction in the mass of the catalyst negatively affects the adsorption process of the contaminant material, thus decreasing the removal efficiency in each cycle, as shown in Figure 12, depicting the removal efficiency for the five cycles.

XRD analysis was done after several catalytic cycles to check the structural stability of the $NiFe_3O_4/MgO/Cr_2O_3$ nanocomposite after photocatalytic recycling. The diffraction pattern that came out of this showed that the peak positions didn't change much, no new phases appeared, and the peak intensity didn't change much compared to the original material. This shows that the composite's crystal structure stays the same after being used again, which means that the material stays phase pure and crystalline even when it is used as a photocatalyst. The fact that the main peaks of $NiFe_3O_4$, MgO, and Cr_2O_3 stayed the same shows that the catalyst is chemically and thermally stable, which means it can be used again and again in environmental applications.

The XRD test on the reused $NiFe_3O_4/MgO/Cr_2O_3$ nanocomposite indicates that the diffraction peaks stay in the same place and have the same strength as the new catalyst, as shown in Figure 13. This shows that the crystal structure and phase composition stay the same even after several photocatalytic cycles. The lack of new peaks or significant broadening shows that the composite keeps its structural integrity and crystallinity, which means it can be used again and again for wastewater treatment. Figure 13 expresses the reused XRD pattern for the composite compared to the original XRD.

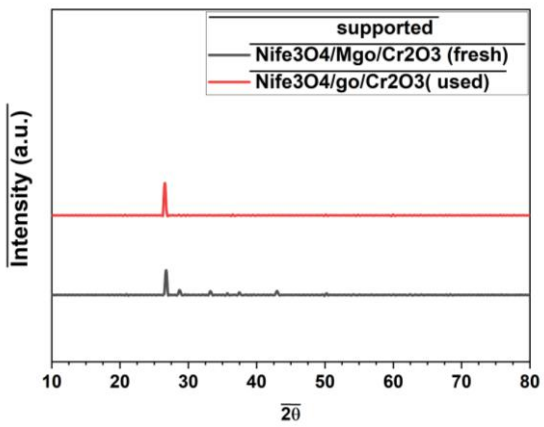

Figure 13. XRD pattern of the composite $NiFe_3O_4/MgO/Cr_2O_3$ after recycling

5. CONCLUSIONS

In this study, a heterogeneous nanocomposite was manufactured from three materials to create an advanced formula that facilitated the photochemical decomposition of MB dye present in wastewater, yielding the following results: The synthesized formula ($NiFe_3O_4/MgO/Cr_2O_3$) for the heterogeneous nanoparticles exhibited an extensive surface area and an elevated degradation rate of the pollutant (MB), compared with the materials used individually. The synthesized compound ($NiFe_3O_4/MgO/Cr_2O_3$) achieved a high removal rate of 97.5%, compared with the separate application of each substance. $NiFe_3O_4$ had a nanoscale removal efficiency of 12%, MgO had a removal efficiency of 72%, and Cr_2O_3 had a removal efficiency of 64%. These results indicated the efficacy of the produced formula. The nanomaterials used featured several advantages: low cost, ease of access and production, and negligible effect on human health.

Future studies will focus on calculating the Turnover Number (TON) to make the evaluation of catalytic performance even stronger. The TON relates the amount of substrate converted to the number of active catalytic sites, which gives a more accurate measure of catalytic efficiency. This characteristic wasn't measured in the current study since there wasn't a clear way to measure active sites. However, including it in future tests will help us learn more about how well the catalyst works and how it compares to others in different reaction cycles. Moreover, real wastewater samples will be used to test the composite material's catalytic ability to see how well it works in more complicated and changing situations. This will assist in figuring out if the material can really be used for environmental cleanup in the actual world and how strong it is.

REFERENCES

[1] Tkaczyk, A., Mitrowska, K., Posyniak, A. (2020). Synthetic organic dyes as contaminants of the aquatic environment and their implications for ecosystems: A review. Science of the Total Environment, 717: 137222. https://doi.org/10.1016/j.scitotenv.2020.137222

[2] Tomar, V., Rusho, M. A., Kumar, S., Madasamy, M., Islam, A.U. (2024). Genetic engineering of microbes for enhanced bioremediation of organic pollutants. African Journal of Biological Sciences, 6(5): 8777-8793. https://doi.org/10.33472/AFJBS.6.5.2024.8777-8793

[3] Hanny N.B. (1976). Treatise on Solid State Chemistry. Springer New York. https://doi.org/10.1007/978-1-4684-8082-5

[4] Al-Baidhani, J.H., Al-Khafajy, Z.H. (2017). Pre-treatment of water by using broken marble and ceramic wastes as up-flow roughing filter media. International Journal of Current Engineering and Technology, 7(1): 74-81.

[5] Mana, M., Ouali, M.S., de Menorval, L.C., Zajac, J.J., Charnay, C. (2011). Regeneration of spent bleaching earth by treatment with cethyltrimethylammonium bromide for application in elimination of acid dye. Chemical Engineering Journal, 174(1): 275-280. https://doi.org/10.1016/j.cej.2011.09.026

[6] Zahra, S., Mazhar, S., Zahra, S., Idrees, H., Hussnain, A. (2022). Synthesis and characterization of magnesium doped titania for photocatalytic degradation of methyl red. Matéria (Rio de Janeiro), 27(1): e202144880. https://doi.org/10.1590/s1517-707620220001.1360

[7] Masekela, D., Hintsho-Mbita, N.C., Sam, S., Yusuf, T. L., Mabuba, N. (2023). Application of BaTiO3-based catalysts for piezocatalytic, photocatalytic and piezo-photocatalytic degradation of organic pollutants and bacterial disinfection in wastewater: A comprehensive review. Arabian Journal of Chemistry, 16(2): 104473.

[8] Vijayalakshmi, P., Shanmugavelan, P., Anisree, S., Mareeswaran, P.M. (2024). Enhanced visible-light Z-scheme photocatalytic degradation of amoxicillin, chlorpyrifos, and methylene blue by Bi2O3/g-C3N4/ZnO nanocomposite. Journal of Materials Research, 39(22): 3103-3125. https://doi.org/10.1557/s43578-024-01445-y

[9] Shakoor, M.H., Shakoor, M.B., Jilani, A., Ahmed, T., Rizwan, M., Dustgeer, M.R., Iqbal, J., Zahid. M., Yong, J.W.H. (2024). Enhancing the photocatalytic degradation of methylene blue with graphene oxide encapsulated g C_3N_4/ZnO ternary composites. ACS Omega, 9(14): 16187-16195. https://doi.org/10.1021/acsomega.3c10172

[10] Swapna, D., Priya, K.J., Sruthi, V., Sunetha, M., Jayashree, R., Himabindu, G., Douglas, S.P. (2024). Studies of ZnO/NiO/MoO_3 ternary nanocomposite as an effective visible light photocatalyst. Asian Journal of Chemistry, 36(12): 2848-2854. https://doi.org/10.14233/ajchem.2024.32718

[11] Wang, J., Shi, P., Han, J., Tian, Y., Yan, Z., Luo, P., Ban, H., Li, Y., Cai, W., Lin, G., Zhai, Z., Li, C. (2025). Investigation of ternary CuZnM (M = Cr, Ce, Zr, Al) catalysts in CO_2 hydrogenation for methanol synthesis. Catalysts, 15(3): 250. https://doi.org/10.3390/catal15030250

[12] Singh, S., Joe, A., Ghotekar, S., Kumar, G., Lokhande, P.E., Kumar, D., Hossain, K., Pant, G. (2024). Synthesis, characterization, and application of ternary composite of CdS/MoS_2/reduced graphene oxide for photocatalytic degradation of sunset dye. Desalination and Water Treatment, 317: 100137. https://doi.org/10.1080/19443994.2024.100137

[13] Doña-Rodríguez, J.M., Pulido Melián, E. (2021). Nano-photocatalytic materials: Possibilities and challenges. Nanomaterials, 11(3): 688. https://doi.org/10.3390/nano11030688

[14] Du, S., Lian, J., Zhang, F. (2022). Visible light-responsive N-doped TiO2 photocatalysis: Synthesis, characterizations, and applications. Transactions of Tianjin University, 28(1): 33-52. https://doi.org/10.1007/s12209-021-00303-w

[15] Hu, Y. L., Zhao, Z., Jiang, J., Huang, Y., Ji, H., Zhu, D., Zhang, L., Zhan, L., Wu, Y., Zhang, Y., Wu, K., Yang, Y., Chai, T., Wu, S., Song, G.L. (2025). Highly oxidative GaN:ZnO@α-Ga2O3 heterostructure as a visible-light-driven, round-the-clock photocatalyst for dye degradation and disinfection. Journal of Materials Chemistry A, 13: 7739-7757. https://doi.org/10.1039/d4ta09029b

[16] Mazurenko, J., Sijo, A. K., Kaykan, L., Kotsyubynsky, V., Gondek, Ł., Zywczak, A., Marzec, M., Vyshnevskyi, O. (2025). Synthesis and characterization of copper ferrite nanoparticles for efficient photocatalytic degradation of organic dyes. Journal of Nanotechnology, 2025(1): 8899491. https://doi.org/10.1155/jnt/8899491

[17] Shi, C., Kang, F., Zhu, Y., Teng, M., et al. (2023). Photoreforming lignocellulosic biomass for hydrogen production: Optimized design of photocatalyst and photocatalytic system. Chemical Engineering Journal, 452: 138980. https://doi.org/10.1016/j.cej.2022.138980

[18] Fosso-Kankeu, E., Pandey, S., Ray, S.S. (2020). Photocatalysts in Advanced Oxidation Processes for Wastewater Treatment. John Wiley & Sons.

[19] Gautam, S., Agrawal, H., Thakur, M., Akbari, A., Sharda, H., Kaur, R., Amini, M. (2020). Metal oxides and metal organic frameworks for the photocatalytic degradation: A review. Journal of Environmental Chemical Engineering, 8(3): 103726. https://doi.org/10.1016/j.jece.2020.103726

[20] Nipa, S.T., Akter, R., Raihan, A., Rasul, S.B., et al. (2022). State-of-the-art biosynthesis of tin oxide nanoparticles by chemical precipitation method towards photocatalytic application. Environmental Science and Pollution Research, 29(8): 10871-10893. https://doi.org/10.1007/s11356-021-17933-1

[21] Inderan, V., Ahmad, N.A.S., Zaidi, N.A.M., Isa, N., Kamis, W.Z.W., Lee, H.L., Raseetha, S. (2023). Hydrothermal synthesis of co and pd doped tin oxide nanorods and their photocatalytic degradation of polypropylene. Malaysian Journal of Analytical Sciences, 27(1): 54-62. https://www.researchgate.net/publication/369184853

[22] Hastuti, S., Martini, T., Wibowo, A.H., Fitriana, D., Zuhara, W., Mutma'inah, H., Putri, R.I. (2025). Removal of heavy metals: Pb(II), Ni(II) and Cd(II) by Fe3O4@SiO2-TMPDT adsorbent prepared from rice husk ash. ALCHEMY Jurnal Penelitian Kimia, 21(1): 53. https://doi.org/10.20961/alchemy.21.1.91934.53-63

[23] Sun, B., Wang, N., Hu, W. (2021). Synthesis of Novel NiFe2O4/Fe3O4Nanotube arrays as flexible negative electrodes for Supercapacitor Applications. IOP Conference Series: Earth and Environmental Science, 639: 012029. https://doi.org/10.1088/1755-1315/639/1/012029

[24] Jabbar, Z.H., Ebrahim, S.E. (2021). Synthesis, characterization, and photocatalytic degradation activity of core/shell magnetic nanocomposites (Fe3O4@SiO2@Ag2WO4@Ag2S) under visible light irradiation. Optical Materials, 122: 111818. https://doi.org/10.1016/j.optmat.2021.111818

[25] Ren, H., Lv, K., Liu, W., Li, P., Zhang, Y., Lv, Y. (2022). Deep-eutectic-solvent-assisted synthesis of a Z-scheme $BiVO_4$/BiOCl/S,N-GQDS heterojunction with enhanced photocatalytic degradation activity under visible-light irradiation. Micromachines, 13(10): 1604. https://doi.org/10.3390/mi13101604

[26] Park, K., Kittelson, D.B., McMurry, P.H. (2004). Structural properties of diesel exhaust particles measured by Transmission Electron Microscopy (TEM): Relationships to particle mass and mobility. Aerosol Science and Technology, 38(9): 881-889. https://doi.org/10.1080/027868290505189

[27] Almalih, R.J. (2024). Introduction to Fourier Transform Infrared Spectroscopy (FTIR). https://www.researchgate.net/publication/385974233.

[28] Quy, B.M., Thu, N.T.N., Xuan, V.T., Hoa, N.T.H., Linh, N.T.N., Tung, V.Q., Le, V.T.T., Thao, T.T., Ngan, N.T.K., Tho, P.T., Hung, N.M., Ha, L.T. (2025). Photocatalytic degradation performance of a chitosan/ZnO-Fe_3O_4 nanocomposite over cationic and anionic dyes under visible-light irradiation. RSC Advances, 15(3): 1590-1603. https://doi.org/10.1039/d4ra08262a

[29] Sukoviene, A., Ali, S., Jagminas, A., Ramanavicius, S. (2025). Magnetic cobalt and other types of ferrite nanoparticles: Synthesis aspects and novel strategies for application in wastewater treatment (Review). Applied

Sciences, 15(2): 857. https://doi.org/10.3390/app15020857
[30] Le, G.H., Thanh, D.A., Pham, T.T.T., Tran, Q.V., Dao, N.N., Nguyen, K.T., Quan, T.T.T. (2025). Synthesis of Z-scheme Ag4V2O7/Ag3VO4/GO nanocomposites for photocatalytic degradation of DDT under visible light. RSC Advances, 15(9): 7078-7089. https://doi.org/10.1039/d5ra00134j
[31] Al Saady, S.H., Ebrahim, S.E. (2024). Efficient photocatalytic degradation of methylene blue using magnetic CoFe2O4@CuO@Ag3VO4 nanocomposite. International Journal of Design and Nature and Ecodynamics, 19(6): 1837-1846. https://doi.org/10.18280/ijdne.190601
[32] Zha, R., Nadimicherla, R., Guo, X. (2015). Ultraviolet photocatalytic degradation of methyl orange by nanostructured TiO_2/ZnO heterojunctions. Journal of Materials Chemistry A, 2015(3): 6565-6574. https://doi.org/10.1039/C5TA00764J
[33] Zhang, L., Li, H., Liu, Y., Tian, Z., Yang, B., Sun, Z., Yan, S. (2014). Adsorption-photocatalytic degradation of methyl orange over a facile one-step hydrothermally synthesized TiO_2/ZnO–NH_2–RGO nanocomposite. RSC Advances, 4(89): 48703-48711. https://doi.org/10.1039/C4RA09227A
[34] Dai, J., Wu, Y., Yao, Y., Zhang, B. (2025). ZnO/TiO_2 composites for degradation of methyl orange by low-power irradiation. Science Progress, 108(1). https://doi.org/10.1177/00368504251322606